Colloids and Surfaces B: Biointerfaces 202 (2021) 111685

Contents lists available at ScienceDirect

Colloids and Surfaces B: Biointerfaces

journal homepage: www.elsevier.com/locate/colsurfb

Interaction of graphene oxide with artificial cell membranes: Role of anionic phospholipid and cholesterol in nanoparticle attachment and membrane disruption

Yiping Feng [a,b,c,*], Yijian Zhang [a], Guoguang Liu [a], Xitong Liu [d,**], Shixiang Gao [c]

[a] Guangzhou Key Laboratory Environmental Catalysis and Pollution Control, Guangdong Key Laboratory of Environmental Catalysis and Health Risk Control, School of Environmental Science and Engineering, Institute of Environmental Health and Pollution Control, Guangdong University of Technology, Guangzhou 510006, China
[b] Department of Environmental Health and Engineering, Johns Hopkins University, Baltimore, MD 21218-2686, United States
[c] State Key Laboratory of Pollution Control and Resource Reuse, School of the Environment, Nanjing University, Nanjing, Jiangsu 210023, China
[d] Department of Civil and Environmental Engineering, The George Washington University, Washington, D.C. 20052, United States

ARTICLE INFO

Keywords:
Graphene oxide
Artificial cell membranes
Membrane disruption
Dye leakage
Lipid bilayer

ABSTRACT

A mechanistic understanding of the interaction of graphene oxide (GO) with cell membranes is critical for predicting the biological effects of GO following accidental exposure and biomedical applications. We herein used a quartz crystal microbalance with dissipation monitoring (QCM-D) to probe the interaction of GO with model cell membranes modified with anionic lipids or cholesterol under biologically relevant conditions. The attachment efficiency of GO on supported lipid bilayers (SLBs) decreased with increasing anionic lipid content and was unchanged with varying cholesterol content. In addition, the incorporation of anionic lipids to the SLBs rendered the attachment of GO partially reversible upon a decrease in solution ionic strength. These results demonstrate the critical role of lipid bilayer surface charge in controlling GO attachment and release. We also employed the fluorescent dye leakage technique to quantify the role of anionic lipids and cholesterol in vesicle disruption caused by GO. Notably, we observed a linear correlation between the amount of dye leakage from the vesicles and the attachment efficiencies of GO on the SLBs, confirming that membrane disruption is preceded by GO attachment. This study highlights the non-negligible role of lipid bilayer composition in controlling the physicochemical interactions between cell membranes and GO.

1. Introduction

The unique physiochemical properties of graphene oxide (GO) have enabled its diverse applications including energy storage, water purification, and drug delivery [1–5]. The release of GO into the environment during the production and use of GO-containing consumer products can lead to potential negative effects on biological systems [6]. GO has been shown to exhibit cytotoxicity to mammalian cells by causing damage to cell membranes [7–9]. Recently, studies have shown that the direct contact between GO and cell membranes is a critical process that initiates the various cytotoxicity pathways [7,10–12]. Therefore, an investigation into the nonspecific interactions of GO with cell membranes will help better understand its cytotoxicity mechanisms and potential risks to human health.

Artificial phospholipid membranes including supported lipid bilayers (SLBs) and lipid vesicles (liposomes) are useful models to study the interactions of engineered nanomaterials (ENMs) with cell membranes [13–15]. Artificial membranes allow for identifying the key components of membranes in controlling ENM-membrane interactions via systematically changing their composition, which is difficult to achieve using living cells [13,16]. SLBs are useful platforms to study the attachment of ENMs onto lipid membranes [17–21], and lipid vesicles can be used to investigate the disruption of the membranes by ENMs [14,19,22–24]. Our previous study demonstrated that the deposition of GO on 1, 2-dioleoyl-sn-glycero-3-phosphocholine (DOPC) SLBs strongly depends on solution chemistry [18]. Ip et al. [25] employed a dye

* Corresponding author at: Guangzhou Key Laboratory Environmental Catalysis and Pollution Control, Guangdong Key Laboratory of Environmental Catalysis and Health Risk Control, School of Environmental Science and Engineering, Institute of Environmental Health and Pollution Control, Guangdong University of Technology, Guangzhou 510006, China.
** Corresponding author.
E-mail addresses: ypfeng@gdut.edu.cn (Y. Feng), xitongliu@gwu.edu (X. Liu).

https://doi.org/10.1016/j.colsurfb.2021.111685
Received 6 December 2020; Received in revised form 1 March 2021; Accepted 6 March 2021
Available online 9 March 2021

leakage assay and showed that the disruption of zwitterionic vesicles by graphene-based materials depends on the oxidation level of the materials. Zucker et al. [26] demonstrated that GO and chemically reduced GO disrupt DOPC vesicles through a lipid-extraction mechanism.

Most of the existing studies employed model membranes that are composed of homogeneous, single-component phospholipid bilayers [18,19,24,26], which lack the complexity of actual cell membranes. Eukaryotic cell membranes contain a mixture of phospholipids, sphingolipids, membrane proteins, and sterols [27–29]. These components play important biological roles and control the physicochemical properties of the membranes. Melby and co-workers showed that the presence of peripheral membrane proteins strongly impacts ENM interaction with model membranes [30]. Currently, we still have very limited understanding of how anionic phospholipids and cholesterol influence ENM-membrane interactions, specifically the propensity and reversibility of ENM attachment as well as the severity of membrane disruption. As an essential component of eukaryotic cell membranes, anionic lipids impart negative charge to the membranes [31]. The negative charge on cell membranes is required for various biological activities such as binding and activation of peripheral and transmembrane proteins [31]. Cholesterol also plays important biological functions: it modulates membrane fluidity, maintains membrane mechanical strength, and regulates cation adsorption to membrane [32–35].

The main objective of the current work is to investigate the interaction of GO with model biological membranes with a variation of phospholipid types and the contents of cholesterol. We used a quartz crystal microbalance with dissipation monitoring (QCM-D) to study the kinetics and reversibility of GO deposition on zwitterionic DOPC SLBs as well as SLBs modified with anionic lipids or cholesterol. Compared with AFM imaging which is semi-quantitative [36], QCM-D experiments allows for ultrasensitive detection (ng/cm^2) of GO mass deposition and release from the SLBs. Using the fluorescent dye leakage method, we quantified the impacts of anionic lipids and cholesterol on the disruption of lipid vesicles by GO. This study will pave the way for an improved understanding of the biological impacts of GO on eukaryotic cells.

2. Materials and methods

2.1. Preparation of graphene oxide

Commercially available single-layered GO (SKU-GO-005) was purchased from Graphene Supermarket (Reading, MA, USA). The composition of GO is 79 % carbon and 20 % oxygen. According to the manufacturer specification, at least 80 % of the GO nanosheets are single-layered. The GO stock suspension was prepared by dispersing 8 mg of GO powder in 200 mL deionized (DI) water (18 MΩ cm, Milli-Q system, Millipore, MA) through ultrasonication (Branson B1510, 40 kHz). The obtained suspension was then passed through a 0.2 μm cellulose acetate filter, and the filtrate was collected as the GO stock suspension. The total organic carbon content of the GO stock suspension was determined through combustion catalytic oxidation at 680 °C (TOC-L, Shimadzu, Japan). Tapping mode atomic force microscopy (AFM) imaging was conducted using a Multimode NanoScope (Bruker) to measure the thickness of the GO nanosheets. The hydrodynamic diameter of the prepared GO, which is the diameter of a hypothetical sphere that diffuses at the same rate as the GO nanosheets, was determined to be 165 − 180 nm through dynamic light scattering (DLS, BI-200SM and BI-9000AT, Brookhaven, NY) based on Stokes-Einstein relation [37,38]. GO stock suspension was stored in the dark at 4 °C until use.

2.2. Vesicles preparation

Zwitterionic 1, 2-dioleoyl-sn-glycero-3-phosphocholine (DOPC), 1, 2-dioleoyl-sn-glycero-3-phospho-L-serine (DOPS), and cholesterol were purchased from Avanti Polar Lipids (Alabaster, AL, USA). The chemical structures of lipids and cholesterol are listed in TableS1. DOPC and DOPS provided in chloroform were directly used as the stock solution. Cholesterol powder was dissolved in chloroform to prepare a stock solution. DOPC, DOPS, and cholesterol stock solutions were kept at −20 °C for further use. We prepared three types of vesicles: pure DOPC, DOPS-modified DOPC (denoted as DOPS-DOPC; DOPS molar contents of 5.7 %, 10.8 %, and 19.5 %), and cholesterol-modified DOPC (denoted as cholesterol-DOPC; cholesterol molar contents of 0%, 10 %, 20 %, and 30 %). It should be noted that these molar contents are not meant to mimic the actual composition of cell membranes but rather are used to explore the fundamental roles of anionic lipids and cholesterol on the interactions between nanoparticles and lipid membranes. To prepare these vesicles, desired amounts of lipids and cholesterol were dissolved in chloroform in an Erlenmeyer flask. A thin lipid film at the bottom of the flask was obtained by drying the solution with a gentle nitrogen stream followed by vacuum desiccation for at least 4 h. The dried film was then re-suspended in N-(2-hydroxyethyl)-piperazine-N'-(2-ethanesulfonic acid) (HEPES) buffer (10 mM HEPES, 150 mM NaCl, pH 7.4) to the desired concentration via magnetic stirring for 30 min. The obtained lipid solution was extruded using a mini-extruder (Avanti Polar Lipids) through a polycarbonate membrane (Whatman) with a pore size of 50 nm for 15 times to produce unilamellar DOPS-DOPC vesicles [19]. Cholesterol-DOPC vesicles were prepared via extrusion through a 100-nm pore size polycarbonate membrane for 21 times [39]. To prepare vesicles for electrophoretic mobilities (EPMs) measurements, the lipid film was hydrated in a 0.2 mM $NaHCO_3$ solution in lieu of HEPES buffers [19]. The prepared vesicles were stored in a nitrogen atmosphere at 4 °C. All vesicles were used within 4 days after preparation. The EPMs of GO and vesicles were measured with a ZetaPALS (Brookhaven Instruments Corp., Holtsville, NY, USA) under physiologically relevant solution chemistries in 100 mM NaCl or 1 mM $CaCl_2$ at pH 7.2 [40,41]. Three samples were measured at each condition and ten measurements were conducted for each sample.

2.3. Deposition and release study using QCM-D

The interactions of GO with the modified SLBs were monitored using a QCM-D system (Q-Sense E4, Västra Frölunda, Sweden) with a 4-sensor chamber. Silica-coated 5 MHz AT-cut quartz crystal sensors (QSX303, Q-Sense) were used for QCM-D measurements. Before use, the silica-coated sensors and QCM-D flow modules were thoroughly cleaned using procedures described in the supplementary material. For all QCM-D experiments, the flow rate was maintained at 0.1 mL min^{-1} using a high-precision multichannel dispenser (ISM935C, Ismatec SA, Zürich, Switzerland) and the temperature was maintained at 25 ± 0.2 °C. Before being introduced into the chamber of QCM-D, the electrolyte solutions were degassed through ultrasonication (Branson 5510R-DTH, output power 135 W, frequency 40 kHz) for 10 min.

For all deposition and release experiments, the normalized frequency and dissipation signals at the third overtone ($f_{(3)}$ and $D_{(3)}$, respectively) were monitored. A baseline was obtained by introducing DI water until the change of normalized frequency was less than 0.2 Hz in a period of 10 min [42]. Next, vesicles were deposited on the surface of the silica-coated crystal sensor to form a continuous SLB [19]. The background electrolyte of interest was then introduced. Once a stable baseline was obtained, a GO suspension (2.5 mg L^{-1}) prepared in the same electrolyte solution was introduced into the chamber to initiate GO deposition. To investigate the release of GO from the SLBs, electrolyte solutions with lower ionic strength (i.e., 0.5 mM NaCl) were sequentially introduced to flush the deposited GO.

We use the rate of frequency shift to represent the deposition rate [42]. The deposition kinetics of GO on SLBs was quantified using the attachment efficiency, α, which was calculated from the deposition rates in the initial 10 min [42,43]:

$$\alpha = \frac{d\Delta f_{(3)}/dt}{(d\Delta f_{(3)}/dt)_{fav}} \quad (1)$$

where $d\Delta f_{(3)}/dt$ represents the deposition rate on SLB, and $(d\Delta f_{(3)}/dt)_{fav}$ represents the deposition rate under favorable condition which was achieved by modifying a silica-coated sensor with a positively charged poly-L-lysine (PLL) layer [19,42,43].

2.4. Dye leakage experiment

Vesicles encapsulated with fluorescent dye were prepared according to previous studies [18,24,26]. Briefly, a dried lipid film was hydrated in HEPES buffer (20 mM HEPES, 150 mM NaCl, pH 7.4) containing 50 mM 5(6)-carboxyfluorescein (CF, J&K, China). After being stirred for 30 min, the re-suspended lipids were extruded through a polycarbonate membrane (Whatman) with a pore size of 100 nm for 21 times to enable the formation of unilamellar vesicles. Next, the untrapped CF was removed via dialysis (100–500 Da molecular weight cutoff) in 20 mM HEPES buffer for 12 h. Using the malachite green method [44], the lipid concentration in the prepared vesicles was determined to be 0.6 mM. The average hydrodynamic diameter of the prepared vesicles was determined as 123–132 nm via DLS experiments. The vesicles were used within 4 days after preparation.

Dye-leakage experiments were performed by mixing dye-encapsulated vesicles with GO in 4-mL cuvettes. The vesicle stock solution was diluted with 20 mM HEPES buffer to obtain a phospholipid concentration of 20 μM. The initial vesicle solution showed a low background fluorescence intensity due to the self-quenching effect of the encapsulated CF dye at high concentration (> 10 mM) [26]. After GO was added into the cuvette at a final concentration of 0–40 mg/L, dye-leakage was monitored by measuring the fluorescence intensity of the solutions over time using a Horiba FlouroMax-4 fluorescence spectrophotometer at excitation and emission wavelengths of 490 and 517 nm, respectively. The time-dependent CF dye leakage was normalized by Eq. (2):

$$L(t) = \frac{I_t - I_0}{I_{max} - I_0} \quad (2)$$

where $L(t)$ is CF leakage ratio, I_t is the time-dependent fluorescence intensity, I_0 is the fluorescence intensity before the addition of GO, and I_{max} is the maximum fluorescence intensity upon complete vesicle rupture induced by the addition of 32 mM Triton X-100 after 120 min.

3. Results and discussion

3.1. Electrokinetic characterization of GO and vesicles

Atomic force microscopy (AFM) imaging (Fig.S1a) indicates that the GO was single layered with thicknesses of ca. 1.0–1.5 nm [45,46], and the size distribution analysis showed most GO sheets had lateral dimension of 50–650 nm (Fig.S1b). The transmission electron microscopy (TEM) image of the GO is presented in Fig.S1c. The TEM image shows that GO has flake-like shape. EPM measurements (Fig.S2) shows that GO was negatively charged under different ionic strengths at pH 7.2 owing to the abundant carboxylic groups on the surface [47]. GO became less negatively charged with increasing NaCl concentration from 0.5 mM to 100 mM due to the screening of surface charge [38]. Moreover, the less negative EPMs of GO at higher $CaCl_2$ concentration (1 mM $CaCl_2$) was attributed to charge screening effect as well as the charge neutralization through binding of Ca^{2+} ions to the carboxyl groups on GO [19,37,38,48].

Fig. 1 shows the EPMs of the three types of vesicles. The DOPC vesicles were slightly negatively charged (–0.30 × 10^{-8} m^2/Vs) at pH 7.2 and 100 mM NaCl. At 1 mM $CaCl_2$, the vesicles were slightly positively charged (0.24 × 10^{-8} m^2/Vs) due to adsorption of Ca^{2+} to the phosphate groups in the lipids [19]. With an increase in the content of anionic phospholipid DOPS, the EPMs of DOPS-DOPC vesicles became more negative (Fig. 1a). At a DOPS content of 19.5 %, the EPMs of the vesicles were –2.33 × 10^{-8} m^2/Vs and –1.4 × 10^{-8} m^2/Vs in 100 mM NaCl and 1 mM $CaCl_2$, respectively. The increase in negative charge with increasing DOPS content is attributed to the negatively charged head group in DOPS (Table S1). Fig. 1b shows that the addition of cholesterol did not significantly change the charge of DOPC vesicles at 100 mM NaCl or 1 mM $CaCl_2$ at pH 7.2 ($p > 0.05$, one way *ANOVA* test), consistent with a previous study [39].

3.2. Deposition kinetics of GO on modified supported lipid bilayers (SLBs)

The DOPS-DOPC and cholesterol-DOPC vesicles were flowed over silica-coated sensors to form modified SLBs. Fig.S3 displays the real-time frequency and dissipation changes (Δf and ΔD) during the formation of the modified SLBs. Generally, Δf_{final} value of ca. –25 Hz and a ΔD value of ca. 0.2 × 10^{-6} indicated the formation of a complete and continuous SLBs on a silica-coated crystal surface [49,50]. We hence calculated Δf_{final} and ΔD_{final} values inFig.S3 and found that the Δf_{final} and ΔD_{final} values for various DOPS-DOPC (Fig.S4a and c) or cholesterol-DOPC (Fig. S4band d) SLBs were similar to the values reported in previous studies for the formation of complete SLBs [49,51]. To further confirm the formation of SLBs on silica, we conducted SEM imaging of pure, DOPS-modified, or cholesterol-modified DOPC vesicles on a glass substrate. The images show the formation of continuous SLBs on glass for all three vesicles in the field of view (Fig. S5), consistent with our QCM-D results. For the cholesterol-DOPC SLBs formed on silica-coated crystals, we also measured the contents of cholesterol in SLBs using the total cholesterol assay kit (Nanjing Jincheng, China). The results in Fig.

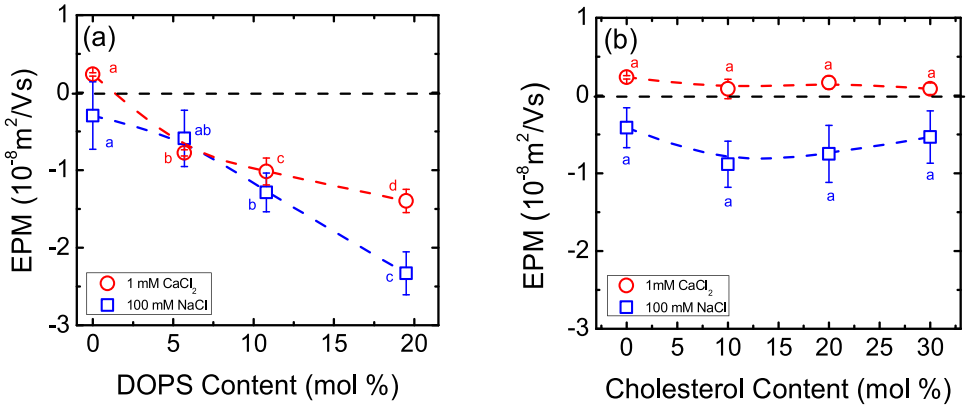

Fig. 1. EPMs of (a) DOPS-DOPC vesicles with DOPS molar percentage ranging from 0 to 19.5 %, and (b) cholesterol-DOPC vesicles with cholesterol molar percentage ranging from 0 to 30 %, at 100 mM NaCl or 1 mM $CaCl_2$, pH 7.2. Error bars represent standard deviations (n = 3). Data points with same letter in same color are not significantly different from one another based on ANOVA test, $p > 0.05$.

S6indicate that cholesterol has been successfully incorporated into the SLBs.

The attachment efficiencies for the deposition of GO on modified SLBs are presented in Fig. 2. An increase in DOPS content from 0 to 19.5 mol% resulted in a decrease in GO deposition in both NaCl and $CaCl_2$ due to the increase in the electrostatic repulsion between DOPS-DOPC SLBs and GO (Fig. 2a). The decrease of attachment efficiency of GO deposition at 1 mM $CaCl_2$ was less significant than at 100 mM NaCl. This can be attributed to that the decrease in EPMs of vesicles with increasing DOPS content was less significant in $CaCl_2$ than in NaCl (Fig. 1a) and that Ca^{2+} ions can bridge the functional groups of GO (e.g., carboxyl groups) and DOPS (e.g., phosphate groups) [43,52].

Different from DOPS, the incorporation of cholesterol in the DOPC SLBs did not significantly change ($p > 0.05$, one-way *ANOVA* test) the attachment efficiencies of GO deposition under the employed solution chemistries (Fig. 2b). It is well recognized that electrical double layer (EDL), hydrophobic, and van der Waals (vdW) interactions play important roles in nanoparticle interactions with membranes [13,29,53,54]. Fig. 1b indicates that the electrostatic interaction between GO and cholesterol-DOPC SLBs did not change appreciably with increasing cholesterol contents. The Hamaker constant for phospholipid/cholesterol mixtures is lower than that for sole phospholipid [55]. The zwitterionic heads of DOPC SLBs facing the aqueous solution are hydrophilic; because cholesterol is more hydrophobic (logKow estimated as 8.86 [56]), the addition of cholesterol is expected to increase the hydrophobicity of the SLBs [57]. Additionally, a computational study revealed that graphene nanosheets preferentially absorbed onto cholesterol in cell membranes via hydrophobic interactions [58]. As such, the inclusion of cholesterol is expected to decrease the vdW attraction between GO and lipid bilayers but increase the hydrophobic attraction. These two opposing effects likely cancel out and result in unchanged attachment efficiency.

3.3. Irreversibility of GO deposition

We investigated the release of GO from pure DOPC, DOPS-DOPC, and cholesterol-DOPC SLBs upon changing solution chemistry. Fig. 3 presents the frequency response when GO deposited on the SLBs at 100 mM NaCl was subsequently rinsed with electrolyte solutions with decreasing ionic strength (i.e. 0.5 mM NaCl and DI water). The pH was maintained at 7.2 throughout the deposition and release experiments. We also monitored the frequency shifts associated with a change in electrolyte concentration by flowing the same electrolyte solutions without GO in separate QCM-D modules (labeled as Buffer Control). The frequency changes associated with rinsing deposited GO with 0.5 mM NaCl were 2.84 and 2.89 Hz on pure DOPC and cholesterol-DOPC SLBs, respectively. Since these frequency shifts are similar to that associated with the buffer effect of 2.89 Hz, GO was not released from pure DOPC and cholesterol-DOPC SLBs. In comparison, the frequency shift resulting from rinsing deposited GO on the DOPS-DOPC SLBs (3.69 Hz) was greater than the buffer effect (2.89 Hz) but less than that corresponding to complete release (4.53 Hz), indicating that GO was released partially from the DOPS-DOPC SLBs.

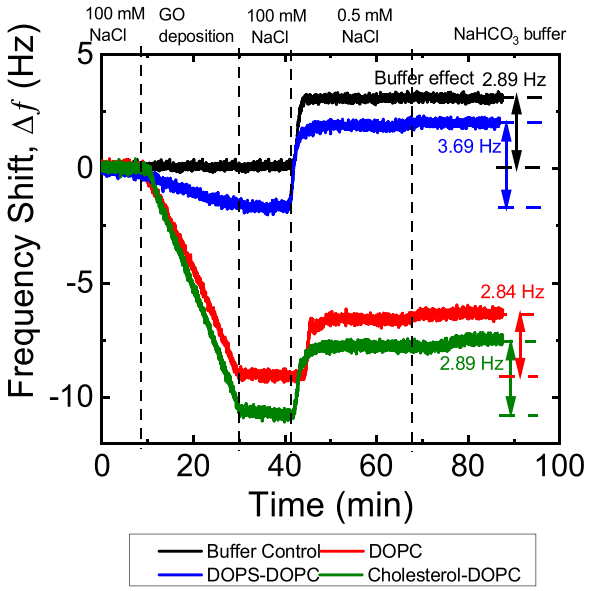

Fig. 3. Frequency shifts during the deposition of GO on DOPC, DOPS-DOPC (with DOPS molar content of 10.8 %), and cholesterol-DOPC (with cholesterol molar content of 30 %) SLBs at 100 mM NaCl and release of GO from SLBs at 100 mM NaCl, 0.5 mM NaCl and 0.2 mM $NaHCO_3$ buffer, all at pH 7.2.

Since the geometry of our QCM-D system does not allow for deposition in the secondary energy minimum [59], GO is expected to deposit in the primary energy minimum prior to release. Ruckenstein and Prieve [60] showed that the remobilization of colloids from the primary energy minimum can be modeled by accounting for EDL interaction, vdW interaction, and Born repulsion. Using this framework, Yi and Chen [59] showed that the energy barrier for release of deposited colloids is reduced with increasing EDL repulsion. As such, the partial GO release from DOPS-DOPC SLBs is likely attributed to the additional negative charge imparted by DOPS and an associated decrease in the magnitude of energy barrier to colloidal release. Our results imply that the deposition of GO on mixed-phospholipid bilayers can be partially reversible upon a change in solution chemistry (e.g., after ingestion of water), which can be an important mechanism for the transport of GO between different biological compartments.

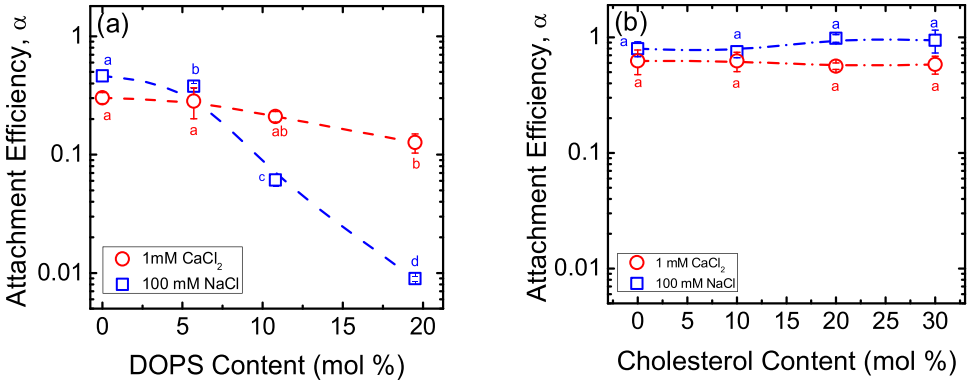

Fig. 2. Attachment efficiencies of GO on (a) DOPS-DOPC SLBs with DOPS molar percentage ranging from 0 to 19.5 %, and (b) cholesterol-DOPC SLBs with cholesterol molar percentage ranging from 0 to 30 %, at 100 mM NaCl or 1 mM $CaCl_2$, pH 7.2. Error bars represent standard deviations (n = 2). Data points with same letter in same color are not significantly different from each other based on ANOVA test, $p > 0.05$.

3.4. Disruption of modified vesicles by GO deposition

The disruption of vesicles induced by GO was examined through dye leakage assay. Fig. S7 presents the time-dependent CF dye leakage ratio from DOPC vesicles, $L(t)$, upon the exposure of GO at various concentrations (0–40 mg/L). The blank sample (only DOPC vesicles in HEPES buffer) showed a minimal increase (7.9 %) in CF dye leakage within 2 h, indicating that CF dye-encapsulated vesicles were stable under the experimental conditions. When GO was introduced into the DOPC vesicle suspension, a rapid and significant increase in CF dye leakage was observed. For example, the addition of GO at 2 and 40 mg/L resulted in 13.6 % and 79.0 % dye leakage, respectively, after 2 h incubation. After subtracting the background/blank sample (Fig. S8a), we found that the CF dye leakage at 120 min ($L_{120\ min}$) from DOPC vesicles was positively correlated to GO concentration (Fig. S8b), indicating that GO deposition induced transient vesicle disruption instead of continuous release [26].

Next, we investigated the disruption of DOPS-DOPC and cholesterol-DOPC vesicles by GO. In the absence of GO, the DOPS and cholesterol modified vesicles were stable with < 10 % dye release (Fig. S9). After subtracting this background, we calculated the time-dependent dye leakage from DOPS-DOPC (Fig. 4) and cholesterol-DOPC (Fig. 5) vesicles caused by GO. Fig. 4a showed the CF dye leakage from DOPS-DOPC vesicles over a range of DOPS molar content from 0 to 19.5 % as a function of time. As DOPS content was increased, $L_{120\ min}$ was gradually decreased, which follows the same trend as the deposition of GO on DOPS-DOPC SLBs (Fig. 2a). We further plotted the dye leakage with attachment efficiencies of GO on DOPS-DOPC SLBs (Fig. 4b). Remarkably, CF dye leakage at 120 min ($L_{120\ min}$) from DOPS-DOPC vesicles was linearly correlated to attachment efficiencies of GO on the SLBs ($R^2 = 0.99997$). This observation is in accordance with the prevalent view that deposition of GO onto SLBs is a critical and necessary step to initiate membrane damage [13].

Fig. 5 presents CF dye leakage kinetics from cholesterol-DOPC vesicles and the $L_{120\ min}$ values over a range of cholesterol molar content from 0 to 30 %. The $L_{120\ min}$ values were not significantly different between vesicles with varying cholesterol contents (one-way ANOVA test, $p > 0.05$) (Fig. 5a). Accordingly, no linear correlation between $L_{120\ min}$ and the attachment efficiencies of GO deposition was observed on cholesterol-DOPC SLBs ($R^2 = 0.004$, Fig. 5b). These results highlight the complex roles that cholesterol might play in modulating GO-SLB interactions. For example, cholesterol in SLBs can interact with GO through hydrophobic interactions, resulting in the extraction of cholesterol and disruption of lipid bilayer [58,61,62]. Additionally, cholesterol can also enhance lipid membrane fluidity, which accommodates vesicle deformation [63,64]. Future studies, particularly molecular simulations, on the role of cholesterol in vesicle disruption will help elucidate these mechanisms.

4. Conclusions

In this study, we prepared multi-component model membranes containing zwitterionic lipids, anionic lipids, and cholesterol to mimic eukaryotic cell membranes. Increasing anionic lipids contents in the model membranes decreased the attachment efficiency of GO, highlighting the important role of electrostatics in controlling GO deposition. In comparison, the incorporation of cholesterol results in a negligible change in membrane surface charge and GO attachment. While the attachment of GO was largely irreversible on zwitterionic lipid bilayers with and without cholesterol, the inclusion of anionic lipids in the bilayers results in partial GO release upon elusion with DI water. Using the dye leakage test, we show that disruption of vesicles induced by GO decreased with increasing anionic lipids content, and the extent of disruption was linearly correlated with the attachment efficiency of GO on the lipid bilayers. We also show that the extent of membrane disruption by GO was not correlated with cholesterol content, likely due to the ability of cholesterol to impact both hydrophobicity and fluidity of the lipid membranes. Overall, our results demonstrate the non-negligible role of anionic lipids and cholesterol in controlling the physicochemical interaction of GO with cell membranes. Our findings also highlight the need for further development of model membranes that are more representative of biological membranes.

Data availability

The authors are unable or have chosen not to specify which data has been used.

CRediT authorship contribution statement

Yiping Feng: Writing - review & editing, Project administration, Funding acquisition. **Yijian Zhang:** Data curation, Methodology, Validation. **Guoguang Liu:** Resources, Supervision. **Xitong Liu:** Formal analysis, Methodology, Validation, Writing - review & editing. **Shixiang Gao:** Resources, Supervision.

Declaration of Competing Interest

The authors declare that they have no known competing financial interests or personal relationships that could have appeared to influence

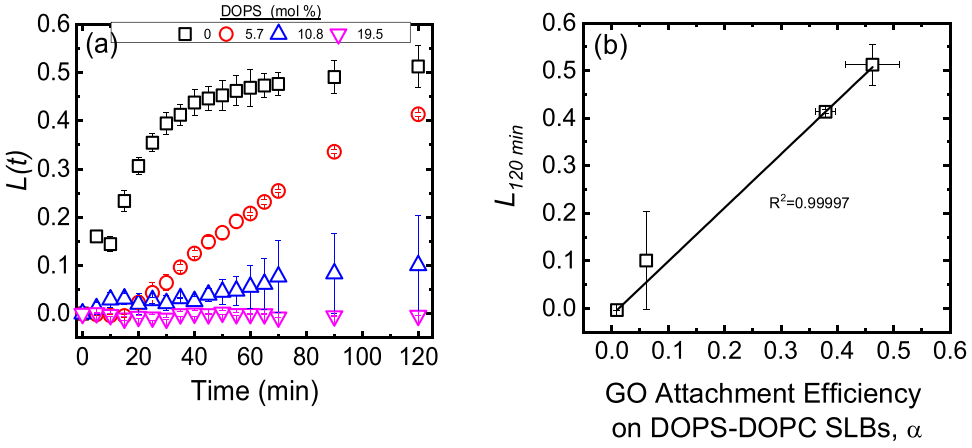

Fig. 4. (a) CF dye leakage kinetics from DOPS-DOPC vesicles with DOPS molar percentage ranging from 0 to 19.5 %, (b) the correlation between CF dye leakage at 120 min ($L_{120\ min}$) from DOPS-DOPC vesicles and attachment efficiencies of GO on DOPS-DOPC SLBs. Experiments were performed with GO at 20 mg/L, 150 mM NaCl, pH 7.4 (20 mM HEPES buffer). Error bars represent standard deviations (n = 3). Data with different letters indicate significant difference, $p < 0.05$.

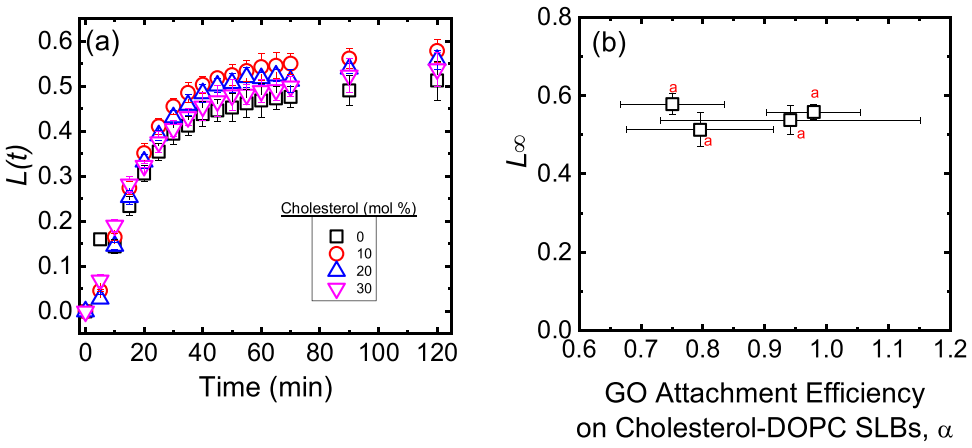

Fig. 5. (a) CF dye leakage kinetics from cholesterol-DOPC vesicles, (b) the correlation between $L_{120\ min}$ from various cholesterol-DOPC vesicles and attachment efficiencies of GO on cholesterol-DOPC SLBs. Experiments were performed with GO at 20 mg/L, 150 mM NaCl, pH 7.4 (20 mM HEPES buffer). Error bars represent standard deviations (n = 3). Data with same letter indicates no significant difference, $p > 0.05$.

the work reported in this paper.

Acknowledgments

We acknowledge funding from the National Natural Science Foundation of China (21707019), and the Graduate Student's Innovative Practice Program of Guangdong Province (pdjh2019b0157) to support the work at Guangdong University of Technology, and Y.F. acknowledges funding support from the China Scholarship Council for the research conducted with Kai Loon Chen's group at Johns Hopkins University.

Appendix A. Supplementary data

Supplementary material related to this article can be found, in the online version, at doi:https://doi.org/10.1016/j.colsurfb.2021.111685.

References

[1] X.M. Sun, Z. Liu, K. Welsher, J.T. Robinson, A. Goodwin, S. Zaric, H.J. Dai, Nano-graphene oxide for cellular imaging and drug delivery, Nano Res. 1 (3) (2008) 203–212.
[2] Y.W. Zhu, S. Murali, W.W. Cai, X.S. Li, J.W. Suk, J.R. Potts, R.S. Ruoff, Graphene and graphene oxide: synthesis, properties, and applications, Adv. Mater. 22 (46) (2010), 5226-5226.
[3] K.P. Loh, Q.L. Bao, G. Eda, M. Chhowalla, Graphene oxide as a chemically tunable platform for optical applications, Nat. Chem. 2 (12) (2010) 1015–1024.
[4] M. Hu, B.X. Mi, Enabling graphene oxide nanosheets as water separation membranes, Environ. Sci. Technol. 47 (8) (2013) 3715–3723.
[5] Y. Jiang, Q. Zeng, P. Biswas, J.D. Fortner, Graphene oxides as nanofillers in polysulfone ultrafiltration membranes: shape matters, J. Membrane Sci. 581 (2019) 453–461.
[6] J. Zhao, Z.Y. Wang, J.C. White, B.S. Xing, Graphene in the aquatic environment: adsorption, dispersion, toxicity and transformation, Environ. Sci. Technol. 48 (17) (2014) 9995–10009.
[7] K. Yang, Y.J. Li, X.F. Tan, R. Peng, Z. Liu, Behavior and toxicity of graphene and its functionalized derivatives in biological systems, Small 9 (9-10) (2013) 1492–1503.
[8] K.H. Liao, Y.S. Lin, C.W. Macosko, C.L. Haynes, Cytotoxicity of graphene oxide and graphene in human erythrocytes and skin fibroblasts, ACS Appl. Mater. Inter. 3 (7) (2011) 2607–2615.
[9] Y.L. Chang, S.T. Yang, J.H. Liu, E. Dong, Y.W. Wang, A.N. Cao, Y.F. Liu, H.F. Wang, In vitro toxicity evaluation of graphene oxide on A549 cells, Toxicol. Lett. 200 (3) (2011) 201–210.
[10] O. Akhavan, E. Ghaderi, Toxicity of graphene and graphene oxide nanowalls against bacteria, ACS Nano 4 (10) (2010) 5731–5736.
[11] S.B. Liu, T.H. Zeng, M. Hofmann, E. Burcombe, J. Wei, R.R. Jiang, J. Kong, Y. Chen, Antibacterial activity of graphite, graphite oxide, graphene oxide, and reduced graphene oxide: membrane and oxidative stress, ACS Nano 5 (9) (2011) 6971–6980.
[12] F. Perreault, A.F. de Faria, S. Nejati, M. Elimelech, Antimicrobial properties of graphene oxide nanosheets: why size matters, ACS Nano 9 (7) (2015) 7226–7236.
[13] K.L. Chen, G.D. Bothun, Nanoparticles meet cell membranes: probing nonspecific interactions using model membranes, Environ. Sci. Technol. 48 (2) (2014) 873–880.
[14] A.M. Farnoud, S. Nazemidashtarjandi, Emerging investigator series: Interactions of engineered nanomaterials with the cell plasma membrane; What have we learned from membrane models? Environ. Sci-Nano 6 (1) (2019) 13–40.
[15] W. Jiang, Q. Wang, X. Qu, L. Wang, X. Wei, D. Zhu, K. Yang, Effects of charge and surface defects of multi-walled carbon nanotubes on the disruption of model cell membranes, Sci. Total Environ. 574 (2017) 771–780.
[16] E.S. Melby, A.C. Mensch, S.E. Lohse, D.H. Hu, G. Orr, C.J. Murphy, R.J. Hamers, J. A. Pedersen, Formation of supported lipid bilayers containing phase-segregated domains and their interaction with gold nanoparticles, Environ. Sci-Nano 3 (1) (2016) 45–55.
[17] K.H. Jacobson, I.L. Gunsolus, T.R. Kuech, J.M. Troiano, E.S. Melby, S.E. Lohse, D. Hu, W.B. Chrisler, C.J. Murphy, G. Orr, F.M. Geiger, C.L. Haynes, J.A. Pedersen, Lipopolysaccharide density and structure govern the extent and distance of nanoparticle interaction with actual and model bacterial outer membranes, Environ. Sci. Technol. 49 (17) (2015) 10642–10650.
[18] X.T. Liu, K.L. Chen, Interactions of graphene oxide with model cell membranes: probing nanoparticle attachment and lipid bilayer disruption, Langmuir 31 (44) (2015) 12076–12086.
[19] P. Yi, K.L. Chen, Interaction of multiwalled carbon nanotubes with supported lipid bilayers and vesicles as model biological membranes, Environ. Sci. Technol. 47 (11) (2013) 5711–5719.
[20] Z. Xia, A. Woods, A. Quirk, I.J. Burgess, B.L. Lau, Interactions between polystyrene nanoparticles and supported lipid bilayers: impact of charge and hydrophobicity modification by specific anions, Environ. Sci-Nano 6 (6) (2019) 1829–1837.
[21] N. Yousefi, N. Tufenkji, Probing the interaction between nanoparticles and lipid membranes by quartz crystal microbalance with dissipation monitoring, Front. Chem. 4 (2016) 46.
[22] P.R. Leroueil, S.A. Berry, K. Duthie, G. Han, V.M. Rotello, D.Q. McNerny, J. R. Baker, B.G. Orr, M.M.B. Holl, Wide varieties of cationic nanoparticles induce defects in supported lipid bilayers, Nano Lett. 8 (2) (2008) 420–424.
[23] C. Corredor, W.C. Hou, S.A. Klein, B.Y. Moghadam, M. Goryll, K. Doudrick, P. Westerhoff, J.D. Posner, Disruption of model cell membranes by carbon nanotubes, Carbon 60 (2013) 67–75.
[24] B.Y. Moghadam, W.C. Hou, C. Corredor, P. Westerhoff, J.D. Posner, Role of nanoparticle surface functionality in the disruption of model cell membranes, Langmuir 28 (47) (2012) 16318–16326.
[25] A.C.F. Ip, B.W. Liu, P.J.J. Huang, J.W. Liu, Oxidation level-dependent zwitterionic liposome adsorption and rupture by graphene-based materials and light-induced content release, Small 9 (7) (2013) 1030–1035.
[26] I. Zucker, J.R. Werber, Z.S. Fishman, S.M. Hashmi, U.R. Gabinet, X.L. Lu, C. O. Osuji, L.D. Pfefferle, M. Elimelech, Loss of phospholipid membrane integrity induced by two-dimensional nanomaterials, Environ. Sci. Tech. Let. 4 (10) (2017) 404–409.
[27] R. Frost, G.E. Jonsson, D. Chakarov, S. Svedhem, B. Kasemo, Graphene oxide and lipid membranes: interactions and nanocomposite structures, Nano Lett. 12 (7) (2012) 3356–3362.
[28] J.M. Troiano, L.L. Olenick, T.R. Kuech, E.S. Melby, D. Hu, S.E. Lohse, A.C. Mensch, M. Dogangun, A.M. Vartanian, M.D. Torelli, E. Ehimiaghe, S.R. Walter, L. Fu, C. R. Anderton, Z. Zhu, H. Wang, G. Orr, C.J. Murphy, R.J. Hamers, J.A. Pedersen, F. M. Geiger, Direct probes of 4 nm diameter gold nanoparticles interacting with supported lipid bilayers, J. Phys. Chem. C 119 (1) (2015) 534–546.
[29] X.Y. Xiao, G.A. Montano, T.L. Edwards, A. Allen, K.E. Achyuthan, R. Polsky, D. R. Wheeler, S.M. Brozik, Surface charge dependent nanoparticle disruption and deposition of lipid bilayer assemblies, Langmuir 28 (50) (2012) 17396–17403.
[30] E.S. Melby, C. Allen, I.U. Foreman-Ortiz, E.R. Caudill, T.R. Kuech, A.M. Vartanian, X. Zhang, C.J. Murphy, R. Hernandez, J.A. Pedersen, Peripheral membrane

proteins facilitate nanoparticle binding at lipid bilayer interfaces, Langmuir 34 (36) (2018) 10793–10805.
[31] R.N.A.H. Lewis, R.N. McElhaney, Surface charge markedly attenuates the nonlamellar phase-forming propensities of lipid bilayer membranes: calorimetric and P-31-nuclear magnetic resonance studies of mixtures of cationic, anionic, and zwitterionic lipids, Biophys. J. 79 (3) (2000) 1455–1464.
[32] X.L.R. Iraolagoitia, M.F. Martini, Ca^{2+} adsorption to lipid membranes and the effect of cholesterol in their composition, Colloids Surf. B Biointerfaces 76 (1) (2010) 215–220.
[33] S.A. Pandit, S.W. Chiu, E. Jakobsson, A. Grama, H.L. Scott, Cholesterol packing around lipids with saturated and unsaturated chains: a simulation study, Langmuir 24 (13) (2008) 6858–6865.
[34] S.A. Pandit, D. Bostick, M.L. Berkowitz, Complexation of phosphatidylcholine lipids with cholesterol, Biophys. J. 86 (3) (2004) 1345–1356.
[35] I. Reviakine, A. Simon, A. Brisson, Effect of Ca^{2+} on the morphology of mixed DPPC-DOPS supported phospholipid bilayers, Langmuir 16 (4) (2000) 1473–1477.
[36] X. Hu, H. Lei, X. Zhang, Y. Zhang, Strong hydrophobic interaction between graphene oxide and supported lipid bilayers revealed by AFM, Microsc. Res. Techniq. 79 (8) (2016) 721–726.
[37] I. Chowdhury, M.C. Duch, N.D. Mansukhani, M.C. Hersam, D. Bouchard, Colloidal properties and stability of graphene oxide nanomaterials in the aquatic environment, Environ. Sci. Technol. 47 (12) (2013) 6288–6296.
[38] M.G. Elimelech, J. Jia, X. Williams, R.A., Particle Deposition and Aggregation - Measurement, Modelling and Smulation, Butterworth-Heinemann, Oxford, England, 1995.
[39] J. Kurniawan, N.N. Yin, G.Y. Liu, T.L. Kuhl, Interaction forces between ternary lipid bilayers containing cholesterol, Langmuir 30 (17) (2014) 4997–5004.
[40] Y. Yue, F. Huo, S. Lee, C. Yin, J. Yoon, A review: the trend of progress about pH probes in cell application in recent years, Analyst 142 (1) (2017) 30–41.
[41] H.Y.Y. Nyein, W. Gao, Z. Shahpar, S. Emaminejad, S. Challa, K. Chen, H.M. Fahad, L.-C. Tai, H. Ota, R.W. Davis, A wearable electrochemical platform for noninvasive simultaneous monitoring of Ca^{2+} and pH, ACS Nano 10 (7) (2016) 7216–7224.
[42] K.L. Chen, M. Elimelech, Interaction of fullerene (C_{60}) nanoparticles with humic acid and alginate coated silica surfaces: measurements, mechanisms, and environmental implications, Environ. Sci. Technol. 42 (20) (2008) 7607–7614.
[43] I. Chowdhury, M.C. Duch, N.D. Mansukhani, M.C. Hersam, D. Bouchard, Deposition and release of graphene oxide nanomaterials using a quartz crystal microbalance, Environ. Sci. Technol. 48 (2) (2014) 961–969.
[44] M. Petitou, F. Tuy, C. Rosenfeld, A simplified procedure for organic phosphorus determination from phospholipids, Anal. Biochem. 91 (1) (1978) 350–353.
[45] D.C. Marcano, D.V. Kosynkin, J.M. Berlin, A. Sinitskii, Z.Z. Sun, A. Slesarev, L. B. Alemany, W. Lu, J.M. Tour, Improved synthesis of graphene oxide, ACS Nano 4 (8) (2010) 4806–4814.
[46] X.T. Liu, C.X. Yan, K.L. Chen, Adsorption of human serum albumin on graphene oxide: implications for protein corona formation and conformation, Environ. Sci. Technol. 53 (15) (2019) 8631–8639.
[47] Y.P. Feng, X.T. Liu, K.A. Huynh, J.M. McCaffery, L. Mao, S.X. Gao, K.L. Chen, Heteroaggregation of graphene oxide with nanometer- and micrometer-sized hematite colloids: influence on nanohybrid aggregation and microparticle sedimentation, Environ. Sci. Technol. 51 (12) (2017) 6821–6828.
[48] L. Wu, L. Liu, B. Gao, R. Munoz-Carpena, M. Zhang, H. Chen, Z.H. Zhou, H. Wang, Aggregation kinetics of graphene oxides in aqueous solutions: experiments, mechanisms, and modeling, Langmuir 29 (49) (2013) 15174–15181.
[49] N.J. Cho, C.W. Frank, B. Kasemo, F. Hook, Quartz crystal microbalance with dissipation monitoring of supported lipid bilayers on various substrates, Nat. Protoc. 5 (6) (2010) 1096–1106.
[50] R. Richter, A. Mukhopadhyay, A. Brisson, Pathways of lipid vesicle deposition on solid surfaces: a combined QCM-D and AFM study, Biophys. J. 85 (5) (2003) 3035–3047.
[51] T.N. Sut, S. Park, Y. Choe, N.J. Cho, Characterizing the supported lipid membrane formation from cholesterol-rich bicelles, Langmuir 35 (47) (2019) 15063–15070.
[52] C.G. Sinn, M. Antonietti, R. Dimova, Binding of calcium to phosphatidylcholine-phosphatidylserine membranes, Colloids Surf. A Physicochem. Eng. Asp. 282 (2006) 410–419.
[53] R. Michel, M. Gradzielski, Experimental aspects of colloidal interactions in mixed systems of liposome and inorganic nanoparticle and their applications, Int. J. Mol. Sci. 13 (9) (2012) 11610–11642.
[54] L. Renner, T. Osaki, S. Chiantia, P. Schwille, T. Pompe, C. Werner, Supported lipid bilayers on spacious and pH-responsive polymer cushions with varied hydrophilicity, J. Phys. Chem. B 112 (20) (2008) 6373–6378.
[55] R. Rand, V. Parsegian, J. Henry, L. Lis, M. McAlister, The effect of cholesterol on measured interaction and compressibility of dipalmitoylphosphatidylcholine bilayers, Can. J. Biochem. 58 (10) (1980) 959–968.
[56] F. Fornasier, L.M.P. Souza, F.R. Souza, F. Reynaud, A.S. Pimentel, Lipophilicity of coarse-grained cholesterol models, J. Chem. Inf. Model. 60 (2) (2020) 569–577.
[57] A.I. Lamond, Molecular biology of the cell, 4th edition, Nature 417 (6887) (2002), 383-383.
[58] L.Y. Zhang, B.Q. Xu, X.Q. Wang, Cholesterol extraction from cell membrane by graphene nanosheets: a computational study, J. Phys. Chem. B 120 (5) (2016) 957–964.
[59] P. Yi, K.L. Chen, Influence of solution chemistry on the release of multiwalled carbon nanotubes from silica surfaces, Environ. Sci. Technol. 47 (21) (2013) 12211–12218.
[60] E. Ruckenstein, D.C. Prieve, Adsorption and desorption of particles and their chromatographic separation, AIChE J. 22 (2) (1976) 276–283.
[61] K.E. Kitko, T. Hong, R.M. Lazarenko, D. Ying, Y.Q. Xu, Q. Zhang, Membrane cholesterol mediates the cellular effects of monolayer graphene substrates, Nat. Commun. 9 (2018).
[62] N. Bernabo, J. Machado-Simoes, L. Valbonetti, M. Ramal-Sanchez, G. Capacchietti, A. Fontana, R. Zappacosta, P. Palestini, L. Botto, M. Marchisio, P. Lanuti, M. Ciulla, A. Di Stefano, E. Fioroni, M. Spina, B. Barboni, Graphene oxide increases mammalian spermatozoa fertilizing ability by extracting cholesterol from their membranes and promoting capacitation, Sci. Rep. 9 (2019).
[63] M. Sundh, S. Svedhem, D.S. Sutherland, Influence of phase separating lipids on supported lipid bilayer formation at SiO2 surfaces, Phys. Chem. Chem. Phys. 12 (2) (2010) 453–460.
[64] M. Rappolt, M.F. Vidal, M. Kriechbaum, M. Steinhart, H. Amenitsch, S. Bernstorff, P. Laggner, Structural, dynamic and mechanical properties of POPC at low cholesterol concentration studied in pressure/temperature space, Eur. Biophys. J. Biophy. 31 (8) (2003) 575–585.